



Study on a phosphorescent copper(I) complex and its oxygen-sensing performances upon polystyrene and MCM-41 matrixes

Xiao-yong Xu^{a,b,*}, Han-ning Xiao^a, Yi-ming Xu^b, Ming-jun Zhang^b

^a College of Materials Science and Engineering, Hunan University, Changsha 410082, China

^b Center for Functional Materials of Pingxiang, Pingxiang 337055, China

ARTICLE INFO

Article history:

Available online 23 April 2012

Keywords:

Cu(I) complex
Oxygen sensor
Molecular sieve
Polystyrene

ABSTRACT

In this paper, we synthesize a new ligand of 1-ethyl-2-(naphthalen-1-yl)-1H-imidazo[4,5-f][1,10]phenanthroline (Phen-Np-Et) and its corresponding Cu(I) complex of [Cu(Phen-Np-Et)(POP)]BF₄, where POP is bis(2-(diphenylphosphanyl)phenyl) ether. The single-crystal structure, electronic nature and photophysical property of [Cu(Phen-Np-Et)(POP)]BF₄ are discussed in detail. It is found that the yellow emission from [Cu(Phen-Np-Et)(POP)]BF₄ owns a long excited state lifetime of 287 μs under pure N₂ atmosphere. Theoretical calculation on [Cu(Phen-Np-Et)(POP)]⁺ suggests that the emission comes from a triplet metal-to-ligand-charge-transfer excited state. Then, [Cu(Phen-Np-Et)(POP)]BF₄ are doped into two matrixes of polystyrene and MCM-41 to investigate the oxygen-sensing performance. Finally, sensitivity maxima of 9.6 and 3.6 are achieved by the composite nanofibers of [Cu(Phen-Np-Et)(POP)]BF₄/polystyrene and the [Cu(Phen-Np-Et)(POP)]BF₄/MCM-41, respectively. Both samples are highly sensitive toward molecular oxygen, owing to the large surface-area-to-volume ratios of nanofibrous membranes and MCM-41 matrix.

© 2012 Elsevier B.V. All rights reserved.

Introduction

The development of optical sensors has sparked the interest in the synthesis and study on photoluminescent transition metal complexes owing to their promising optical and electrical characters for electro-optical applications [1,2]. Compared with traditional sensors for sensing gases, metal ions and organic matters, optical sensors have low requirement in instrumental implementation and sample preparation. Therefore, research efforts have been devoted to their development regarding their advantages such as easy-to-take, quick and non-destructive characteristics [3,4]. Particularly, many research efforts have been assigned to the development of optical sensors for oxygen detection since the quantification of molecular oxygen is usually an importance problem in various branches of environmental monitoring, chemical industry and medicine, as well as biological and analytical chemistry [5,6].

To allow analyte transportation from surrounding and eliminate self-quenching of optical sensors, sensing molecules are usually chemically grafted or physically attached onto supporting matrixes. Polystyrene and silica-based molecular sieves have shown their virtues such as photodurability in visible spectral region, high surface-area-to-volume ratio and easy loading of sensing molecules,

making themselves potential supporting matrix candidates for optical sensing systems [7]. Consequently, the development of sensing molecules with appropriate emission intensity and energy, long-lived excited state, high photodurability and good compatibility with the supporting matrixes remains to be a challenge.

Owing to their advantages of less toxic, low cost, redundant resource and environmental friendliness, phosphorescent Cu(I) complexes have attracted much research interest as a new class of optoelectrical material. Recently, Zhang and coworkers have reported a series of copper(I) complexes of [Cu(N-N)(P-P)]BF₄ that have been proved to be superior emitters [8–10]. According to Zhang's report, for a typical phosphorescent Cu(I) complex, its highest occupied molecular orbital (HOMO) and HOMO-1 have predominant metal Cu d character, while its lowest unoccupied molecular orbital (LUMO) and LUMO + 1 are essentially π* orbitals localized on the diamine ligand [8]. The photoluminescence corresponds to the lowest triplet T₁ and is thus assigned as a character of metal-to-ligand-charge-transfer ³MLCT [d(Cu) → π*(diamine ligand)]. The excited state corresponding to electronic transition from HOMO to LUMO is thus vulnerable to energy acceptors and surrounding variations [8,10].

In this paper, we report a phosphorescent Cu(I) complex of [Cu(Phen-Np-Et)(POP)]BF₄. Its crystal structure, photophysical property and electronic nature are discussed in detail. In addition, we dope [Cu(Phen-Np-Et)(POP)]BF₄ into a polymer matrix of polystyrene (PS) and a silica molecular sieve of MCM-41, hoping to study and compare the oxygen-sensing performance.

* Corresponding author at: College of Materials Science and Engineering, Hunan University, Changsha 410082, China. Tel.: +86 018970596060.

E-mail address: dreamxxy01@163.com (X.-y. Xu).

Experimental section

A synthetic route for $[\text{Cu}(\text{Phen-Np-Et})(\text{POP})]\text{BF}_4$ and the corresponding composite material of $[\text{Cu}(\text{Phen-Np-Et})(\text{POP})]\text{BF}_4/\text{PS}$ is shown in Scheme 1. POP, $\text{Cu}(\text{BF}_4)_2$, EtBr, silica molecular sieve of MCM-41 and 1-naphthaldehyde (NP-CHO) were purchased from Aldrich Chemical Co. and used without further purifications. The starting material of 1,10-phenanthroline-5,6-dione (referred as Phen-O) was synthesized according to the literature procedure [7,11]. All organic solvents were purified using standard procedures.

Synthesis of diamine ligands

Phen-Np. A typical synthetic route for Phen-Np is described as follows. The mixture of 20 mmol of Phen-O, 22 mmol of Np-CHO, 15.40 g of NH_4Ac and 30 mL of HAc was stirred at 90°C for 4 h. Then, the mixture was poured into cold water and extracted with CH_2Cl_2 . After the evaporation of solvent, the crude product was further purified by recrystallization from EtOH. ^1H NMR (CDCl_3 , 300 MHz) δ [ppm]: 11.62 (s, 1H), 9.13 (m, 2H), 8.79 (m, 1H), 8.54 (m, 1H), 7.94 (m, 3H), 7.72 (m, 1H), 7.63 (m, 1H), 7.56 (m, 4H).

Phen-Np-Et. A typical synthetic route for 1-ethyl-2-(naphthalen-1-yl)-1H-imidazo[4,5-f][1,10]phenanthroline (referred as Phen-Np-Et) is described as follows. The mixture of 20 mmol of NaH and 100 mL of anhydrous *N,N*-dimethylformamide (DMF) was stirred for 1 h, and then, 10 mmol of Phen-Np and 50 mmol of EtBr were added into above solution. The mixture was heated to reflux for 24 h. After cooling, the mixture was poured into cold water and

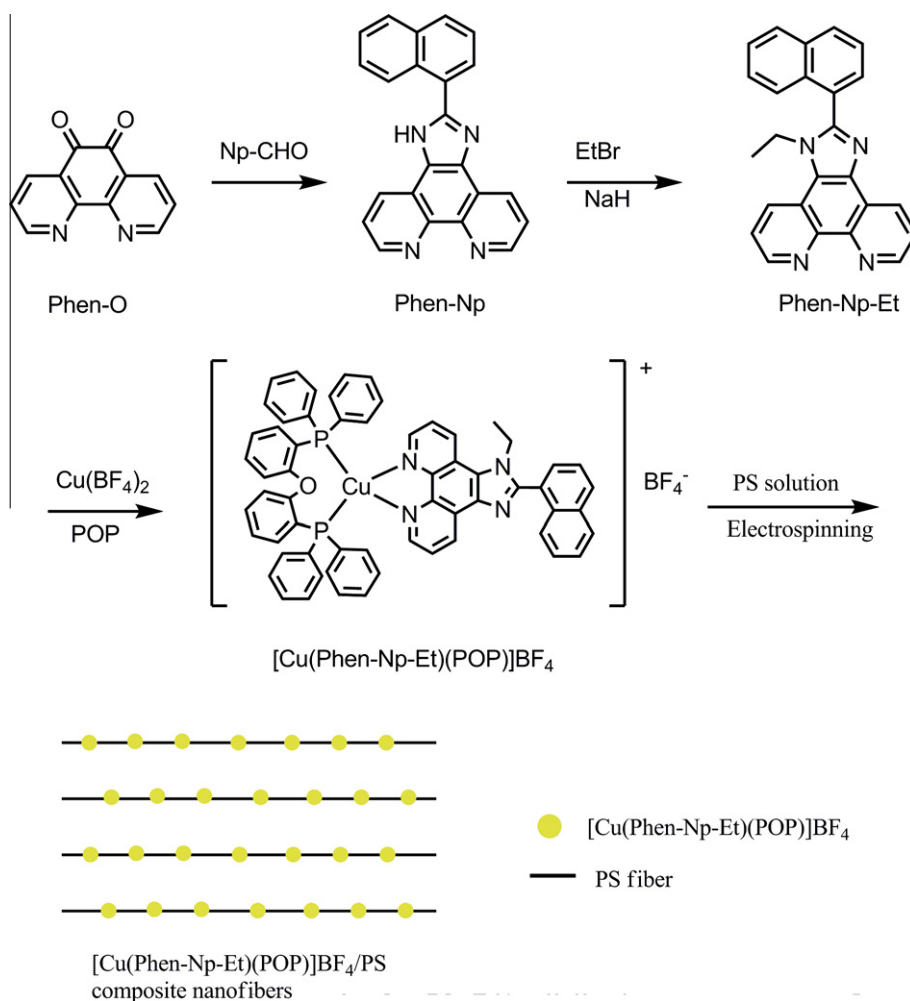
extracted with CH_2Cl_2 . After the evaporation of solvent, the residue was further purified by recrystallization from hot methanol to give the desired product. ^1H NMR (CDCl_3 , 300 MHz) δ [ppm]: 9.17 (m, 2H), 9.09 (d, $J = 4.5$ Hz, 1H), 8.65 (m, 1H), 8.09 (m, 1H), 7.99 (m, 1H), 7.72 (m, 3H), 7.67 (m, 1H), 7.54 (m, 2H), 7.49 (m, 1H), 4.42 (q, 2H), 1.435 (t, 3H).

Synthesis of $[\text{Cu}(\text{Phen-Np-Et})(\text{POP})]\text{BF}_4$

$[\text{Cu}(\text{Phen-Np-Et})(\text{POP})]\text{BF}_4$ was synthesized according to the classic literature procedure [10]. Its identity was confirmed by ^1H NMR, elemental analysis, IR spectrum and single-crystal XRD. ^1H NMR (CDCl_3 , 300 MHz) δ [ppm]: 9.15 (m, 2H), 8.74 (d, $J = 5.4$ Hz, 2H), 8.10 (d, $J = 6.0$ Hz, 1H), 7.98 (d, $J = 6.0$ Hz, 1H), 7.62 (m, 7H), 7.15 (m, 8H), 6.96 (m, 12H), 6.29 (m, 2H), 4.61 (q, 2H), 1.47 (t, 3H). Anal. Calcd for $\text{C}_{61}\text{H}_{46}\text{BCuF}_4\text{N}_4\text{OP}_2$: C, 68.90; H, 4.36; N, 5.27. Found: C, 68.81; H, 4.24; N, 5.35. IR (KBr pellet): ν 3040, 2985, 1587, 1547, 1425, 1249, 1048, 864, 798, 771, 718 cm^{-1} .

Fabrication of $[\text{Cu}(\text{Phen-Np-Et})(\text{POP})]\text{BF}_4/\text{PS}$ composite nanofibers

A typical procedure for the electrospinning composite nanofibers is described as follows. PS with a number-average molecular mass of 100,000 was dissolved in DMF to form a 22 wt.% solution. Then, $[\text{Cu}(\text{Phen-Np-Et})(\text{POP})]\text{BF}_4$ was added into the solution under stirring to form $[\text{Cu}(\text{Phen-Np-Et})(\text{POP})]\text{BF}_4/\text{PS}$ homogeneous solutions. The final solutions were then electrospun to be composite nanofibers of $[\text{Cu}(\text{Phen-Np-Et})(\text{POP})]\text{BF}_4/\text{PS}$. For electrospinning, the



Scheme 1. A synthetic route for $[\text{Cu}(\text{Phen-Np-Et})(\text{POP})]\text{BF}_4$ and $[\text{Cu}(\text{Phen-Np-Et})(\text{POP})]\text{BF}_4/\text{PS}$ composite nanofibers.

mixed solution was placed in a 5 ml glass syringe, with the opening end connected to a plastic needle (inner diameter = 0.6 mm) as the nozzle [12]. The anode terminal of a high-voltage generator was connected to a copper wire inserted into the polymer solution in the glass syringe. A piece of Al foil was used as the collector plate and connected to the grounding electrode. The driving voltage was 18 kV, with the tip-to-target distance of 25 cm.

Fabrication of [Cu(Phen-Np-Et)(POP)]BF₄/MCM-41 composite silica

[Cu(Phen-Np-Et)(POP)]BF₄ was incorporated into mesoporous silica molecular sieve of MCM-41 following the procedure: 1 g of MCM-41 and 60 mg of [Cu(Phen-Np-Et)(POP)]BF₄ were added into 10 mL of dichloromethane, and the mixture was stirred under ambient condition for 24 h. The resulted suspension was filtered to give pale yellow powder. The powder was washed with dichloromethane until the solution was colorless under ultraviolet radiation and then dried under N₂ atmosphere.

Methods and measurements

Density functional theory (DFT) and singlet excitation calculations using time-dependent density functional theory (TD-DFT) were performed on [Cu(Phen-Np-Et)(POP)]⁺ at RB3PW91/SBKJC level. The initial geometry was obtained from its single crystal. All computations were finished by GAMESS software package. The IR spectrum was recorded using a Magna 560 FT-IR spectrophotometer. Excited state lifetimes were obtained with a 355 nm light generated from the Third-Harmonic-Generator pumped, using pulsed Nd:YAG laser as the excitation source. The Nd:YAG laser possesses a line width of 1.0 cm⁻¹, pulse duration of 10 ns and repetition frequency of 10 Hz. A Rhodamine 6G dye pumped by the same Nd:YAG laser was used as the frequency-selective excitation source. All photoluminescence (PL) spectra were measured with a Hitachi F-4500 fluorescence spectrophotometer. UV-Vis absorption spectra were recorded using a Shimadzu UV-3101PC spectrophotometer. Scanning electron microscopy (SEM) image was obtained on a Hitachi S-4800 microscope. Small angle X-ray diffraction (SAXRD) patterns were measured with a Rigaku-Dmax 2500 diffractometer using Cu K α ($\lambda = 0.15405$ nm) radiation at 0.02° (2 θ) scanning step. Fluorescence microscopy image was obtained with a Nikon TE2000-U fluorescence microscopy using mercury lamp as the power supply. ¹H NMR spectra were obtained with a Varian INOVA 300 spectrometer. Elemental analysis was performed on a Carlo Erba 1106 elemental analyzer. Single-crystal data were collected on a Siemens P4 single-crystal X-ray diffractometer with a Smart CCD-1000 detector and graphite-monochromated Mo K α radiation, operating at 50 kV and 30 A at 298 K. All hydrogen atoms were calculated. Oxygen-sensing performances were measured on the basis of steady emission intensity quenching. In the measurement of Stern–Volmer plots, oxygen and nitrogen were mixed at different concentrations via gas flow controls and passed directly into sealed gas chamber. All measurements were carried out in the air at room temperature without being specified.

Results and discussion

Molecular nature of [Cu(Phen-Np-Et)(POP)]BF₄

Single-crystal structure

In Fig. 1, we present the single-crystal structure of [Cu(Phen-Np-Et)(POP)]BF₄, and the key structural parameters are listed in Table 1. The dihedral angle between N–Cu–N and P–Cu–P planes is measured to be 89.62°, which suggests that the Cu(I) center

localizes in a distorted tetrahedral coordination sphere. The two Cu–N bond length values are slightly different from each other and measured to be 2.035 Å and 2.074 Å, respectively. Similar cases have been reported by literature reports, which means that the intermolecular interactions between Cu(I) center and N atoms are slightly different from each other owing to their different electronic nature [9,13]. As for the two Cu–P bonds, their values are quite similar with each other. Both P atoms are found to be ~2.3 Å away from the Cu(I) center, suggesting that the intermolecular interactions between Cu(I) center and P atoms are much similar with each other due to the unique electronic nature of two P atoms. The O atom in POP ligand is measured to be ~2.3 Å away from the Cu(I) center, suggesting that there may be some intermolecular interaction between Cu(I) center and the O atom. However, this distance is much longer than normal chemical bonds and should not be considered as a coordination bond. Literatures on POP-based Cu(I) complexes have also reported examples with similar Cu···O separations [8,9,13].

The N–Cu–N bite angle is measured to be as large as 80.46°, which is comparable with literature values [8,9,13], and this large bite angle is attributed to the static congestion caused by the large dihedral angle between N–Cu–N and P–Cu–P planes (89.62°) as mentioned. On the other side, the P–Cu–P bite angle is measured to be 118.06°. Since POP has a nature bite angle of 102.2° with a flexibility ranging from 86° to 120°, the large P–Cu–P bite angle may suggest a congestion of coordination environment round Cu(I) center [14].

In addition, it can be seen that naphthalene moiety is uncoplanar with Phen ring. The free rotation of naphthalene moiety may compromise the large conjugation system, leading to a strong static hindrance. So, even though there are two large planes of naphthalene moiety and Phen ring within Phen-Np-Et ligand, neither inter- nor inner-molecular π -stacking is observed in [Cu(Phen-Np-Et)(POP)]BF₄ crystal.

Electronic structure

According to literature reports, the MLCT excited state of [Cu(N–N)(P–P)]BF₄ may be vulnerable to energy acceptors and surrounding variations [8,10]. To get a deeper understanding on the electronic structure of [Cu(Phen-Np-Et)(POP)]BF₄, a DFT calculation was

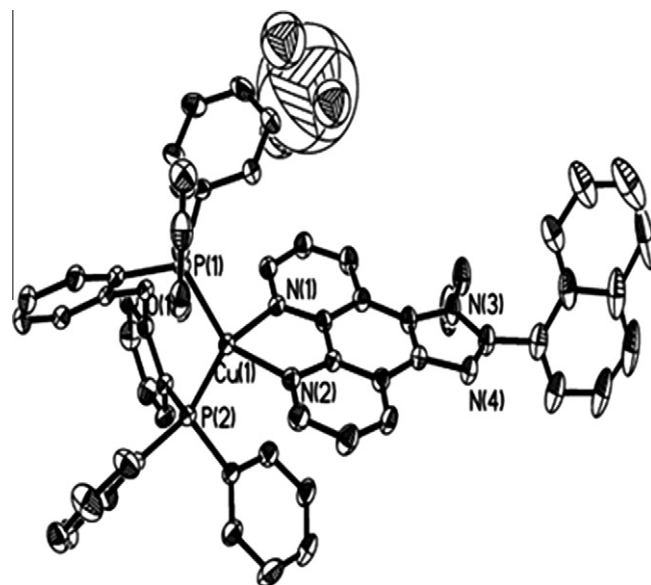


Fig. 1. Molecular structure [Cu(Phen-Np-Et)(POP)]BF₄ obtained from its single crystal. All hydrogen atoms are omitted for clarity.

Table 1
Selected bond lengths (Å) and angles (°) of [Cu(Phen-Np-Et)(POP)]BF₄ obtained from single crystal.

Bond length	(Å)	Bond angle	(°)
Cu(1)–N(1)	2.074	N(1)–Cu–N(2)	80.46
Cu(1)–N(2)	2.035	N(1)–Cu–P(1)	109.14
Cu(1)–P(1)	2.226	N(2)–Cu–P(1)	122.59
Cu(1)–P(2)	2.255	N(1)–Cu–P(2)	104.44
Cu···O	3.063	N(2)–Cu–P(2)	113.11
		P(1)–Cu–P(2)	118.06

performed on the Cu(I) complex, which has been demonstrated to be an effective method to explore the electronic structure of transition metal complexes [8–10]. The percentage compositions of frontier orbitals and the first five singlet excitation of [Cu(Phen-Np-Et)(POP)]⁺ are summarized in Table 2. The graphic presentation of HOMO and LUMO shown in Fig. 2 suggests that HOMO of [Cu(Phen-Np-Et)(POP)]⁺ mainly localizes on Cu(I) center and P atoms, while its LUMO is mainly composed of π^* orbital of Phen-Np-Et, which is consistent with literature report [8–10]. The first electronic transition is assigned as an electronic transition from HOMO to LUMO, which confirms that the onset electronic transition of [Cu(Phen-Np-Et)(POP)]BF₄ is a MLCT one. As shown in Table 2, LUMO is essentially π^* orbital of Phen-Np-Et ligand, and the excited state electron localizing on LUMO may thus be attacked and quenched by energy acceptors such as molecular oxygen, leading to a decrease or even absence of emission intensity.

Photophysical properties of [Cu(Phen-Np-Et)(POP)]BF₄

The UV–Vis absorption spectrum of [Cu(Phen-Np-Et)(POP)]BF₄ in CH₂Cl₂ solution with a concentration of 1×10^{-4} mol/L is shown in Fig. 3, along with those of free Phen-Np-Et ligand and POP ligand for comparison purpose. The absorption spectrum of [Cu(Phen-Np-Et)(POP)]BF₄ is mainly composed of two regions, ending at ~460 nm. After the absorption spectrum comparison between free ligands and [Cu(Phen-Np-Et)(POP)]BF₄, the strong absorption ranging from 220 nm to 325 nm is assigned to ligand $\pi \rightarrow \pi^*$ transitions, while the weak absorption ranging from 350 nm to 450 nm is tentatively attributed to MLCT transitions. After a comparison between absorption spectra of [Cu(Phen)(POP)]BF₄ (Phen = 1,10-phenanthroline) and [Cu(Phen-Np-Et)(POP)]BF₄, the MLCT absorption of [Cu(Phen-Np-Et)(POP)]BF₄ red shifts by ~10 nm, owing to the large coplanar conjugation system in Phen-Np-Et ligand [8]. However, the redshift tendency is limited, which may be caused by the conjugation break between naphthalene moiety and Phen ring, owing to the free rotation of naphthalene moiety as mentioned above.

Table 2
Orbital percentage composition of [Cu(Phen-Np-Et)(POP)]⁺ calculated at RB3LYP/SBKJ level.

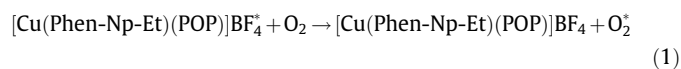
Orbitals/ transition	Composition (%)	Energy (eV)
LUMO + 1(174)	Phen-Np-Et(93.5)	-3.935
LUMO(173)	Phen-Np-Et(84.7) and POP(11.7)	-4.291
HOMO(172)	Cu(28.6) and POP(65.4)	-7.701
HOMO - 1(171)	Cu(26.6) and Phen-Np(58.2) and POP(15.3)	-8.003
HOMO - 2(170)	Cu(22.3) and Phen-Np(65.2) and POP(12.3)	-8.038
HOMO - 3(169)	Cu(34.6) and Phen-Np(21.2) and POP(44.2)	-8.226
S ₀ → S ₁	171 → 173(60.4) and 170 → 173(34.5)	2.7401
S ₀ → S ₂	172 → 173(96.3)	2.8074
S ₀ → S ₃	169 → 173(94.7)	3.0747
S ₀ → S ₄	172 → 174(96.8)	3.1468
S ₀ → S ₅	171 → 174(63.2) and 170 → 174(34.3)	3.2716

[Cu(Phen-Np-Et)(POP)]BF₄ in solid state gives a broad emission band centering at 550 nm as shown in Fig. 4. The emission band shows no vibronic progressions with a full-width-at-half-maximum (FWHM) of 93 nm, which indicates that the emissive state owns a charge-transfer (CT) character. The Stokes shift of [Cu(Phen-Np-Et)(POP)]BF₄ between its absorption edge and emission maximum is calculated to be 90 nm, which is comparable with literature values [8]. This large value suggests that there is an intense structural relaxation that occurs in excited state. The emissive energy of 550 nm is comparable with that of [Cu(Phen)(POP)]BF₄ [8], which means that the energy gap of [Cu(Phen-Np-Et)(POP)]BF₄ is similar with that of [Cu(Phen)(POP)]BF₄ due to naphthalene moiety's inefficient conjugation with Phen ring.

The emission decay curves shown by the inset of Fig. 4 suggest that the excited state of [Cu(Phen-Np-Et)(POP)]BF₄ has a long lifetime of 287 μ s under pure N₂ atmosphere, which identifies the phosphorescence nature of the emission. Bearing above calculation results in mind, we conclude that the emission is generated from ³MLCT excited state. A long-live excited state may give energy acceptors enough time to attack and quench the excited state, favoring sensitivity improvement and instant response [9].

Then, the potential surface crossing (PSC) from higher $\pi \rightarrow \pi^*$ state to lower MLCT state of [Cu(Phen-Np-Et)(POP)]BF₄ is discussed as follows. As shown by the inset of Fig. 4, the emission under pure N₂ atmosphere follows a biexponential decay pattern with $\tau_1 = 380 \mu$ s ($A_1 = 0.642$) and $\tau_2 = 80 \mu$ s ($A_1 = 0.420$), respectively. It is reported that the observation of strong absorption in $\pi \rightarrow \pi^*$ absorption region and a short-lived decay component from $\pi \rightarrow \pi^*$ state than those from MLCT state suggests an efficient PSC from the higher $\pi \rightarrow \pi^*$ state to MLCT state. The absorption spectrum of [Cu(Phen-Np-Et)(POP)]BF₄ shown in Fig. 3 exhibits a strong absorption at $\pi \rightarrow \pi^*$ absorption region. Consequently, τ_2 is assigned to $\pi \rightarrow \pi^*$ decay, and τ_1 is assigned to MLCT decay.

Under pure O₂ atmosphere, the excited state lifetime decreases to 0.2 μ s, which is over 1000 times shorter than that under pure N₂ atmosphere. The largely decreased lifetime suggests that [Cu(Phen-Np-Et)(POP)]BF₄ excited state can be easily quenched by molecular oxygen through a dynamic mechanism described as follows [7]:



where “*” denotes excited state.

Characterization of [Cu(Phen-Np-Et)(POP)]BF₄/PS and [Cu(Phen-Np-Et)(POP)]BF₄/MCM-41

Since it has been above confirmed that [Cu(Phen-Np-Et)(POP)]BF₄ emission is quenched by molecular oxygen, we decide to further explore its oxygen-sensing performance. For practical sensing systems, optical probes should be embedded into supporting matrix to eliminate self-quenching of optical probes and to allow analyte transportation from surrounding. There are also some stringent criteria for supporting matrix to achieve suitable performances [7]. Here, we select PS and MCM-41, which have been proved to be excellent supporting materials for optical sensors, as the supporting matrixes for our primitive research [7,15].

At first, three dopant concentrations of 3.0 wt.%, 3.5 wt.% and 4.0 wt.% are tried to achieve optimal performance. A typical SEM image of the 3.5 wt.% doped sample is shown in Fig. 5a. [Cu(Phen-Np-Et)(POP)]BF₄/PS sample shows smooth and uniform morphology with average diameter of ~500 nm. The fibers are randomly distributed on the substrate without any branch structures, and this unique morphology has been reported to own a large surface-area-to-volume ratio that is two orders of magnitude larger

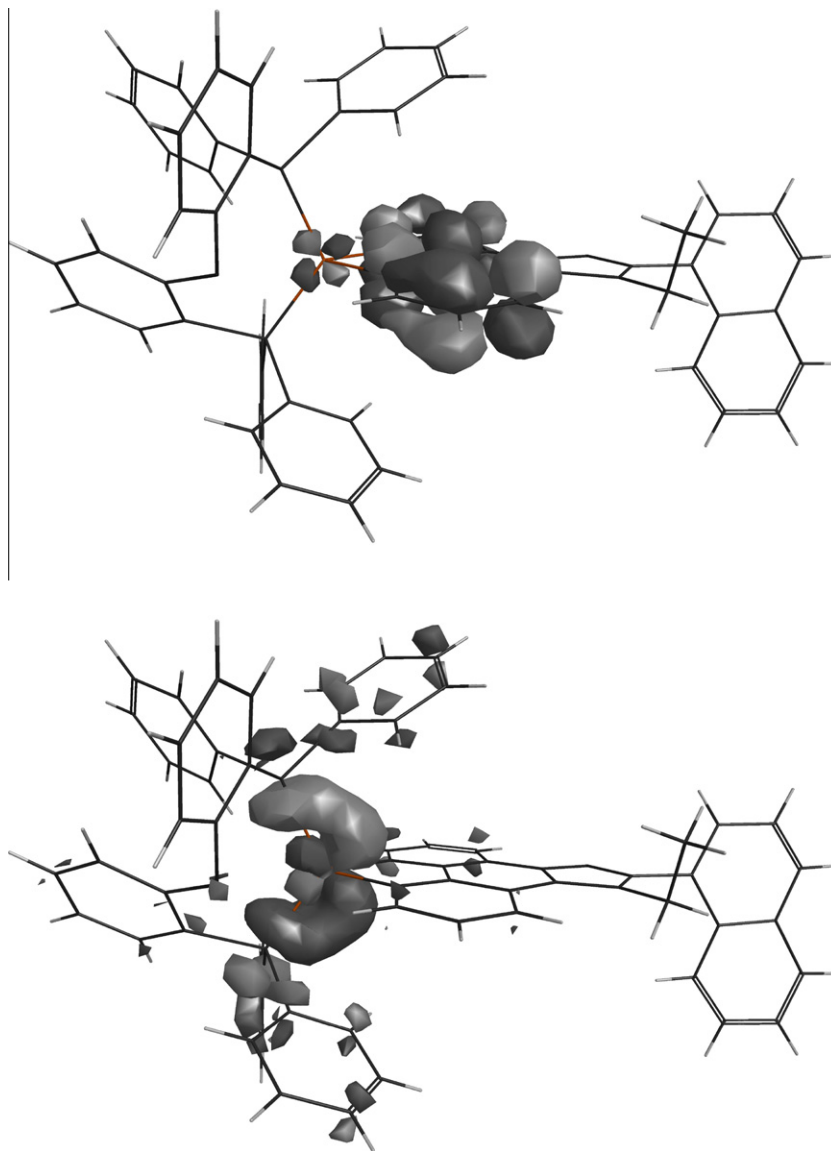


Fig. 2. HOMO (down) and LUMO (up) of [Cu(Phen-Np-Et)(POP)]⁺ calculated at RB3PW91/SBKJ level.

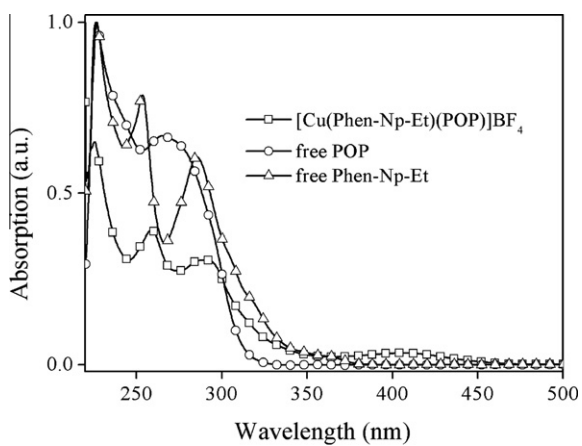


Fig. 3. UV-Vis absorption of Phen-Np, POP and [Cu(Phen-Np-Et)(POP)]BF₄ in CH₂Cl₂ solutions with a concentration of 1×10^{-4} mol/L.

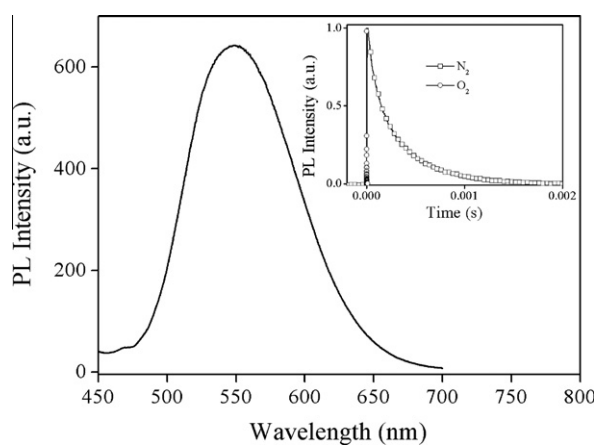


Fig. 4. PL spectrum of [Cu(Phen-Np-Et)(POP)]BF₄ in solid state. Inset: PL intensity decay data of [Cu(Phen-Np-Et)(POP)]BF₄ upon N₂ and O₂ atmosphere.

than that of bulk materials, giving a high diffusion coefficient for rapid response [15]. Correspondingly, the fluorescence

microscopy image of the 3.5 wt.% doped sample exhibits typical yellow emission that is assigned to [Cu(Phen-Np-Et)(POP)]BF₄,

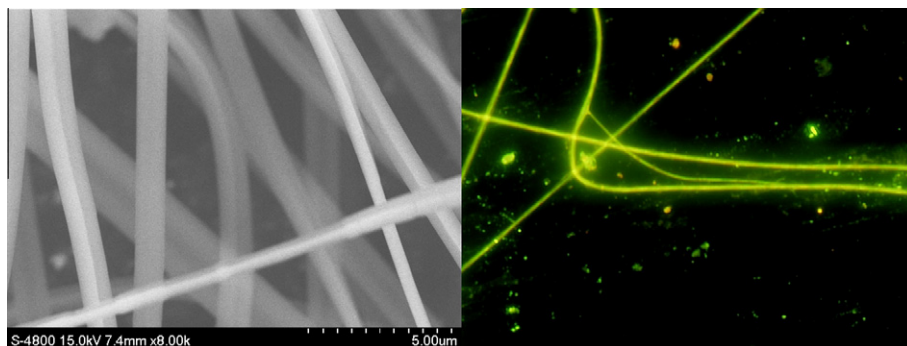


Fig. 5a. SEM (left) and fluorescence microscopy (right) images of the 3.5 wt.% doped sample.

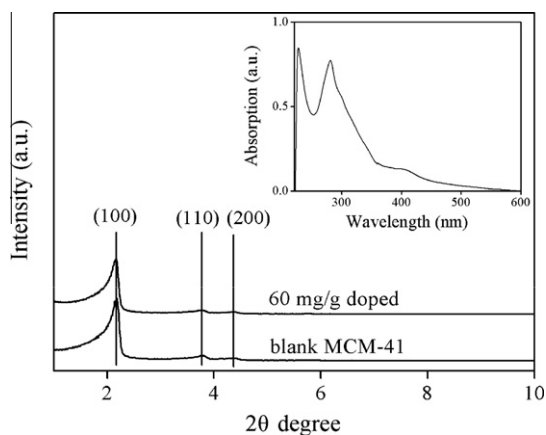


Fig. 5b. SAXRD 1 patterns of blank MCM-41 and [Cu(Phen-Np-Et)(POP)]BF₄/MCM-41. Inset: absorption spectrum of [Cu(Phen-Np-Et)(POP)]BF₄/MCM-41.

suggesting that [Cu(Phen-Np-Et)(POP)]BF₄ has been successfully doped into the composite nanofibers.

To compare the influence of matrix on sensing performances, we also prepare [Cu(Phen-Np-Et)(POP)]BF₄/MCM-41 with optimal doping concentration of 60 mg/g [12,16]. The powder small angle X-ray diffraction (SAXRD) pattern of blank MCM-41 shown in Fig. 5b exhibits three well-resolved broad Bragg reflections of d_{100} , d_{110} and d_{200} , indicating a well-ordered hexagonal mesostructure [9,10]. The well-ordered channels of MCM-41 silica result in a large surface-area-to-volume ratio, making itself a good supporting matrix for rapid response. After the incorporation of [Cu(Phen-Np-Et)(POP)]BF₄, the SAXRD pattern of [Cu(Phen-Np-Et)(POP)]BF₄/MCM-41 is nearly identical with that of blank MCM-41, which means that the well-ordered hexagonal arrangement of channels in MCM-41 remains after the incorporation of [Cu(Phen-Np-Et)(POP)]BF₄. In addition, the absorption spectrum of [Cu(Phen-Np-Et)(POP)]BF₄/MCM-41 shown by the inset of Fig. 5b is similar with that of pure [Cu(Phen-Np-Et)(POP)]BF₄, showing identical absorption characters. It is thus confirmed that [Cu(Phen-Np-Et)(POP)]BF₄ has been successfully doped into MCM-41 matrix.

Oxygen-sensing properties of [Cu(Phen-Np-Et)(POP)]BF₄/PS nanofibers

Sensitivity

The luminescence response of the 3.5 wt.% doped sample under various oxygen concentrations from 0% to 100% with an interval of 10% is shown in Fig. 6. The emission intensity of 538 nm decreases sharply with increasing oxygen concentrations, which means that [Cu(Phen-Np-Et)(POP)]BF₄/PS is highly sensitive toward oxygen. To evaluate the sensing performance, sensitivity is defined as

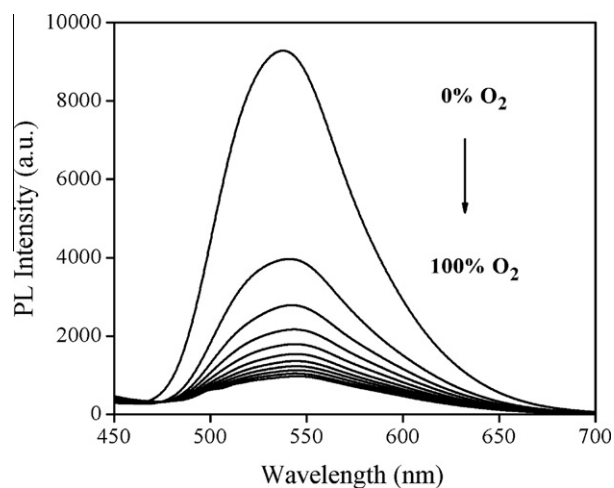


Fig. 6. Emission spectra of the 3.5 wt.% doped sample under various oxygen concentrations from 0% to 100% with an interval of 10%.

I_0/I_{100} , where I_0 is the luminescence intensity under 100% N₂ atmosphere and I_{100} is that under 100% O₂ atmosphere. The sensitivity values are then calculated to be 7.8 for the 3.0 wt.% doped sample, 9.6 for the 3.5 wt.% doped sample and 9.1 for the 4.0 wt.% doped sample, respectively. It is observed that the 3.5 wt.% doped sample owns a higher sensitivity than the others, and we give an explanation as follows. There should be at least two opposite components that control the sensitivity: one is the emission intensity from [Cu(Phen-Np-Et)(POP)]BF₄, and the other is the self-quenching between [Cu(Phen-Np-Et)(POP)]BF₄ molecules. When the dopant concentration is low, the emission is weak, which leads to the low sensitivity of the 3.0 wt.% doped sample. On the other hand, a high dopant concentration may accelerate the self-quenching of [Cu(Phen-Np-Et)(POP)]BF₄ molecules, which also decreases the emission intensity and correspondingly leads to a low sensitivity of the 4.0 wt.% doped sample. The two factors may get balanced in the 3.5 wt.% doped sample, showing the maximum sensitivity of 9.6.

Another finding is that the emission maximum of the 3.5 wt.% doped sample shifts to 538 nm, compared with that of pure [Cu(Phen-Np-Et)(POP)]BF₄ centering at 550 nm. This decreased Stokes shift is tentatively attributed to rigidochromism described as follows. Zhang and coworkers have reported that the structural relaxation that occurs in the excited state of [Cu(N-N)(P-P)]BF₄ decreases the energy content sharply [8–10]. When doped into PS matrix, [Cu(Phen-Np-Et)(POP)]BF₄ molecules are trapped in the rigid grid of PS, and the structural relaxation can thus be effectively suppressed, leading to abovementioned emission spectrum blue shift.

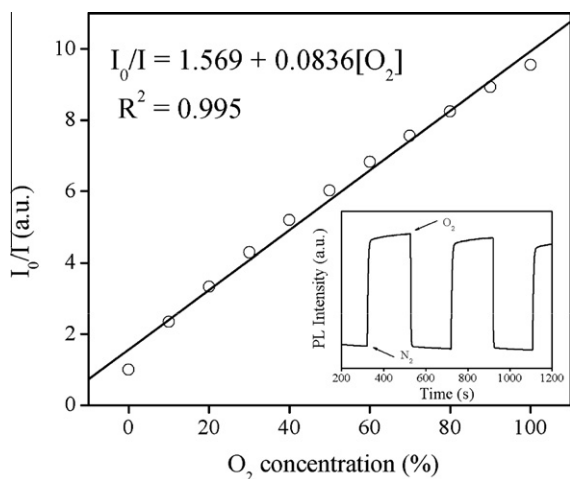


Fig. 7. Stern–Volmer plot of the 3.5 wt.% doped sample under various oxygen concentrations from 0% to 100% with an interval of 10%. Inset: PL intensity responses of the 3.5 wt.% doped sample under periodically varied 100% N₂ and 100% O₂ atmospheres.

Stern–Volmer plot

As for an emission with single-exponential decay pattern, the intensity form of Stern–Volmer equation with dynamic quenching is described as follows [16].

$$I_0/I = 1 + K_{SV}[O_2] \quad (2)$$

where I is steady emission intensity, I_0 denotes the emission intensity at pure N₂ atmosphere, K_{SV} is the Stern–Volmer constant, and $[O_2]$ is O₂ concentration. A plot of I_0/I versus $[O_2]$ should be linear with identical slopes of K_{SV} . The Stern–Volmer plot of the 3.5 wt.% doped sample under various oxygen concentrations is shown in Fig. 7. It can be seen that the plot fits Eq. (2) very well and the quenching curve shows good linear response with increasing oxygen concentrations. We thus come to a conclusion that [Cu(Phen-Np-Et)(POP)]BF₄ molecules localize in a homogeneous micro-environment and are uniformly distributed in PS matrix, leading to a smooth quenching on [Cu(Phen-Np-Et)(POP)]BF₄ excited state.

Response/recovery times and photostability

The PL signal response of the 3.5 wt.% doped sample upon periodically varied 100% N₂ and 100% O₂ atmospheres is shown by the inset of Fig. 7. For comparison convenience, we define 95% response time as the time taken for a sample to lose 95% of its initial emission intensity when changed from 100% N₂ atmosphere to 100% O₂ atmosphere, and 95% recovery time as the time taken to recover 95% if its final emission intensity when changed from 100% O₂ atmosphere to 100% N₂ atmosphere [7,16]. The 3.5 wt.% doped sample owns a response time of 16 s and a recovery time of ~25 s. The instant emission quenching suggests that [Cu(Phen-Np-Et)(POP)]BF₄/PS is highly sensitive toward molecular oxygen. We attribute this character to both [Cu(Phen-Np-Et)(POP)]BF₄'s vulnerable excited state and the large surface-area-to-volume ratio supplied by PS matrix. The recovery time is found to be longer than the response time, which has been explained by the diffusion-controlled dynamic response and recovery behavior of a hyperbolic-type sensor reported by Mills and coworkers [17]. In addition, the maximum emission intensity at pure N₂ atmosphere shows a decrease tendency, which is called photobleaching. This result suggests that PS matrix, however, is limited on protecting [Cu(Phen-Np-Et)(POP)]BF₄ molecules from photodecomposition.

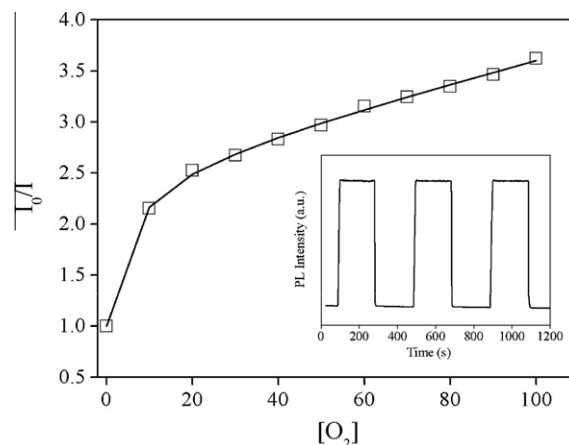


Fig. 8. Stern–Volmer plot of [Cu(Phen-Np-Et)(POP)]BF₄/MCM-41 under various oxygen concentrations from 0% to 100% with an interval of 10%. Inset: PL intensity response under periodically varied 100% N₂ and 100% O₂ atmospheres.

Oxygen-sensing properties of [Cu(Phen-Np-Et)(POP)]BF₄/MCM-41

In order to further improve the photostability, as well as compare the effect of supporting matrix on sensing performance, we decide to dope [Cu(Phen-Np-Et)(POP)]BF₄ into a silica matrix of MCM-41 with an optimal dopant concentration of 60 mg/g [12,16]. The Stern–Volmer plot of [Cu(Phen-Np-Et)(POP)]BF₄/MCM-41 under various oxygen concentrations is shown in Fig. 8. Clearly, the linearity is so poor compared with that of [Cu(Phen-Np-Et)(POP)]BF₄/PS, and the maximum sensitivity is only 3.6. These data suggest that [Cu(Phen-Np-Et)(POP)]BF₄ cannot be uniformly distributed in MCM-41 supporting matrix, and the quenching is ineffective. However, the 60 mg/g doped sample shows a good photodurability, and no obvious photobleaching is observed, as shown by the inset of Fig. 8. Upon pure O₂ atmosphere, the emission is largely quenched, but the emission intensity can always recover to its initial value when the atmosphere changes from 100% O₂ to 100% N₂, suggesting that the sensing system is not suffering from oxidative photobleaching. Thus, we come to a conclusion that PS matrix owns a virtue of uniform distribution, while MCM-41 matrix can offer good protection for sensing probes.

Conclusion

In this paper, we synthesized an oxygen-sensing Cu(I) complex of [Cu(Phen-Np-Et)(POP)]BF₄. Its single-crystal structure, electronic nature and photophysical property are discussed in detail. By doping [Cu(Phen-Np-Et)(POP)]BF₄ into two supporting matrixes of PS and MCM-41, the oxygen-sensing performance is investigated. The composite nanofibers show a maximum sensitivity of 9.6 with good linearity owing to the large surface-area-to-volume ratio of nanofibrous membranes. However, the photodurability is underdeveloped. While the composite silica sample gives a low sensitivity of 3.6 with poor linearity, the photodurability is perfect. All these results suggest that phosphorescent [Cu(Phen-Np-Et)(POP)]BF₄ doped nanofibrous membranes and silica molecular sieves are potential candidates for low-cost and quick-response oxygen-sensing materials. Above conclusion may be useful for the future design of oxygen-sensing materials.

Acknowledgment

This work was supported by Grants from the Science Foundation of Jiangxi Province, China (GJJ12661).

References

- [1] L. Cambot, M. Cantuel, Y. Leydet, G. Jonusauskas, D.M. Bassani, N.D. McClenaghan, *Coord. Chem. Rev.* 252 (2008) 2572–2584.
- [2] D.V. Scaltrito, D.W. Thompson, J.A. O'Callaghan, G.J. Meyer, *Coord. Chem. Rev.* 208 (2000) 243–266.
- [3] G. Zhang, J. Chen, S.J. Payne, S.E. Kooi, J.N. Demas, C.L. Fraser, *J. Am. Chem. Soc.* 129 (2007) 15728.
- [4] A. Gulino, S. Giuffrida, P. Mineo, M. Purrazzo, E. Scamporrino, G. Ventimiglia, M.E. Van der Boom, I. Fragala, *J. Phys. Chem. B* 110 (2006) 16781–16786.
- [5] O.S. Wolfbeis, *Anal. Chem.* 80 (2008) 4269–4283.
- [6] C. Baleizao, S. Nagl, M. Schaferling, M.N. Berberan-Santos, O.S. Wolfbeis, *Anal. Chem.* 80 (2008) 6449–6457.
- [7] B. Lei, B. Li, H. Zhang, L. Zhang, W. Li, *J. Phys. Chem. C* 111 (2007) 11291–11301.
- [8] L. Zhang, S. Yue, B. Li, D. Fan, *Inorg. Chim. Acta* 384 (2012) 225–232.
- [9] L. Yang, J.K. Feng, A.M. Ren, M. Zhang, Y.G. Ma, X.D. Liu, *Eur. J. Inorg. Chem.* 10 (2005) 1867–1879.
- [10] L. Zhang, B. Li, Z. Su, *Langmuir* 25 (2009) 2068–2074.
- [11] L. Zhang, B. Li, *J. Lumin.* 129 (2009) 1304–1308.
- [12] H.Q. Yu, H.W. Song, G.H. Pan, S.W. Li, Z.X. Liu, X. Bai, T. Wang, S.Z. Lu, H.F. Zhao, *J. Lumin.* 124 (2007) 39–44.
- [13] D.G. Cuttell, S.M. Kuang, P.E. Fanwick, D.R. McMillin, R.A. Walton, *J. Am. Chem. Soc.* 124 (2002) 6–7.
- [14] M. Kranenburg, Y.E.M. van der Brugt, P.C.J. Kamer, P.W.N.M. van Leeuwen, *Organometallics* 14 (1995) 3081–3089.
- [15] Y. Wang, B. Li, Y. Liu, L. Zhang, Q. Zuo, L. Shi, Z. Su, *Chem. Commun.* 39 (2009) 5868–5870.
- [16] L. Shi, B. Li, S. Yue, D. Fan, *Sensor Actuat. B: Chem.* 137 (2009) 386–392.
- [17] A. Mills, A. Lepre, *Anal. Chem.* 69 (1997) 4653–4659.